Tunable Metal-Organic Frameworks Enable High Efficiency Cascaded Adsorption Heat Pumps

Authors: Adam J. Rieth[1], Ashley M. Wright[1], Sameer Rao[2], Hyunho Kim[2], Alina D. LaPotin[2], Evelyn N. Wang[2], Mircea Dincă[1]*

Affiliations:

[1]Department of Chemistry, Massachusetts Institute of Technology, 77 Massachusetts Ave. Cambridge, Massachusetts, 02139, United States.

[2]Department of Mechanical Engineering, Massachusetts Institute of Technology, 77 Massachusetts Ave. Cambridge, Massachusetts, 02139, United States.

Summary

Rising global standards of living coupled with the recent agreement to eliminate hydrofluorocarbon refrigerants are creating intense pressure to develop more sustainable climate control systems. In this vein, the use of water as the refrigerant in adsorption heat pumps is highly attractive, but such adsorption systems are constrained to large size and poor efficiency by the characteristics of currently employed water sorbents. Here we demonstrate control of the relative humidity of water uptake by modulating the pore size in a family of isoreticular triazolate metal-organic frameworks. Using this method, we identify a pair of materials with stepped, non-overlapping water isotherms that can function in tandem to provide continuous cooling with a record ideal coefficient of performance of 1.63. Additionally, when used in a single-stage heat pump, the microporous Ni_2Cl_2BBTA has the largest working capacity of any material capable of generating a 25 °C difference between ambient and chiller output.

Introduction

More than 44% of all primary energy in the U.S. residential and commercial sectors is consumed by climate control systems.[1] Globally, as standards of living in the developing world rise, the resultant rapid growth in demand for air conditioning is a major driver of increased worldwide electricity consumption.[2] Thermally-driven cooling cycles, such as adsorption heat pumps (AHPs), can utilize previously wasted energy resources such as engine exhaust, waste heat from power generation, or chemical process heat, resulting in dramatic reductions in primary energy consumption for heating and cooling.[3–5] Interest in AHPs using water as the refrigerant has spiked in light of the recent agreement to phase out hydrofluorocarbons, the refrigerants most commonly employed in conventional vapor compression heat pumps, due to their very high global warming potential.[6–8]

Widespread deployment of AHPs is limited by shortcomings of the currently employed active sorbents, including low water capacity and shallow water uptake step profiles that are not tunable as a function of relative humidity (RH).[3,9–12] These shortcomings result in bulky devices which suffer from low thermal efficiency. In principle, the efficiency of AHP systems, as measured by the coefficient of performance (COP, defined as the cooling energy per unit energy input), could be improved by employing multiple-effect cascaded cycles wherein two or more adsorbent beds are operated in series.[13] Cascaded
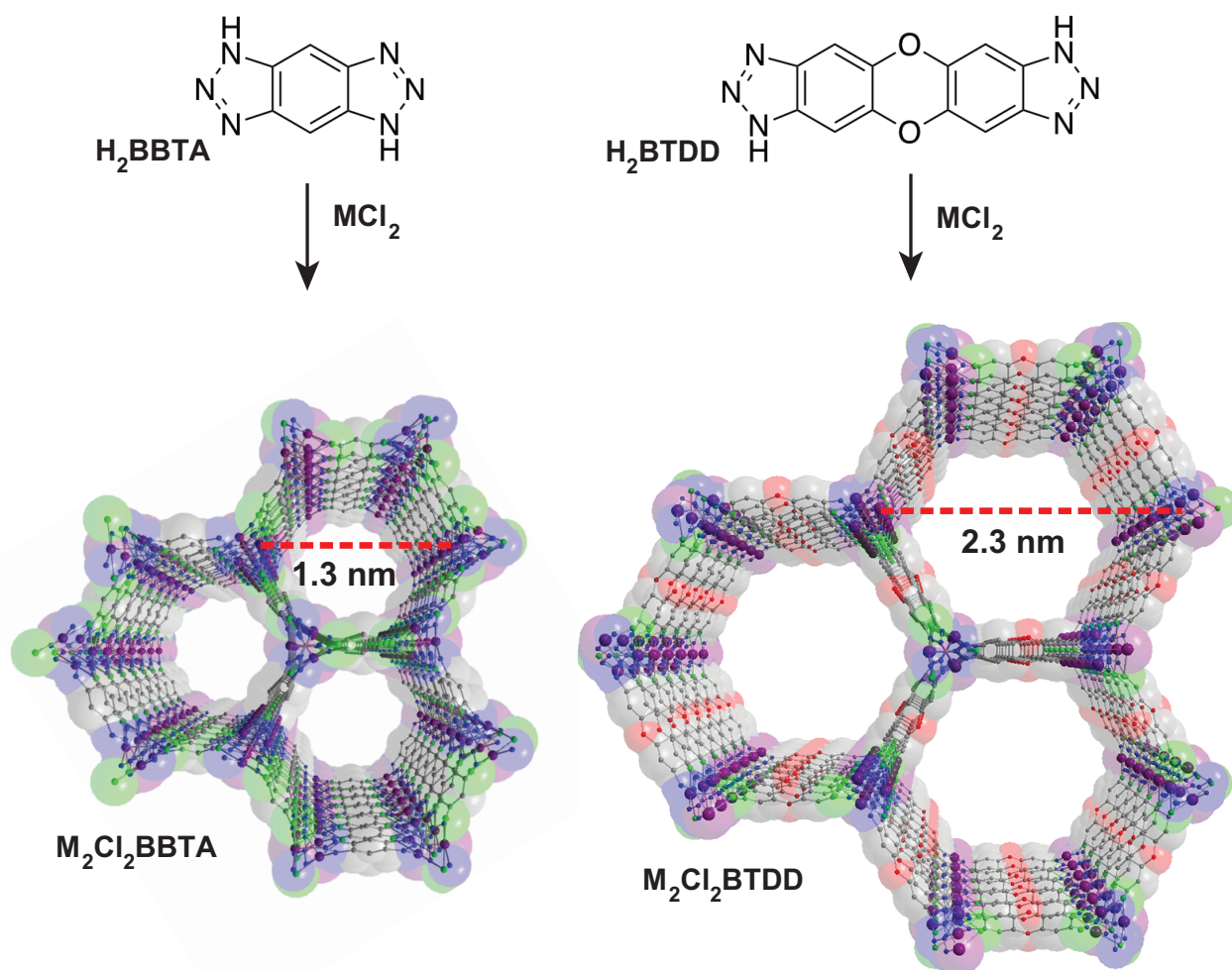
Figure 1: **Synthetic route and structure depiction of M₂Cl₂BBTA and M₂Cl₂BTDD**. C – gray, O – red, N – blue, Cl – green, M – purple. For clarity, H atoms are omitted.

temperature stages allow for the reuse of input thermal energy at progressively lower temperatures in each successive bed, resulting in higher overall efficiency. For instance, a three-stage cascaded AHP using silica gel and activated carbon adsorbents can achieve a superb overall COP of 1, but requires an elevated driving temperature of 220 °C.[14] Further improvements require designing pairs of materials with water uptake steps tailored to fully reuse the excess energy from the high temperature stage with the low temperature stage. Such fine tuning in adsorbent design has not been possible so far.

In view of their recently demonstrated utility as sorbents in AHPs,[4,9,10,15,16] metal-organic frameworks (MOFs) are poised to offer thermodynamically matched material pairs that would enable record performance in cascaded systems. In addition to higher overall capacity, MOFs typically exhibit steeper uptake steps, occurring in a narrow RH range, which directly improve efficiency because cycling between the filled state and the empty state requires a minimal temperature swing.[17] Most importantly for cascaded AHPs, MOFs allow for precise control over the position of water uptake as a function of RH. [11,18–25] This is vital because it determines the maximum temperature difference (lift) an AHP system can produce and defines the required driving temperature to regenerate the sorbent.[9] More hydrophilic sorbents will adsorb water at lower RH, and can produce a

higher lift, but will also require a higher temperature heat source for regeneration because water is adsorbed more strongly. Therefore, the ideal sorbent is one whose hydrophilicity provides enough driving force to achieve the target temperature lift, but is not so high as to decrease thermal efficiency.[9,16]

We recently reported a MOF, Co_2Cl_2BTDD (BTDD = bis(1H-1,2,3-triazolo[4,5-b],[4′,5′-i])dibenzo[1,4]dioxin) whose pore size allows water sorption at the uptake reversibility limit.[16,26] Co_2Cl_2BTDD is the best-performing sorbent for single-stage AHPs capable of a 20 °C lift.[9,16] Here we show that a smaller-pore isoreticular MOF made from the shorter bistriazolate linker 1H,5H-benzo(1,2-d),(4,5-d′)bistriazole (BBTA)[27,28] is significantly more hydrophilic and enables a lift greater than 40 °C, which, in combination with the larger pore system, can enable a record high-efficiency (COP > 1) cascaded double-effect AHP system.

Results

Water vapor adsorption isotherms measured at 298 K for activated samples of M_2Cl_2BBTA (M = Co, Ni, Cu) are shown in **Figure 2**. All three materials exhibit type I isotherms with pore filling at low RH, attributed to coordination of water at the metal nodes, followed by further hydrogen bonding-assisted adsorption until pore saturation. The nickel and cobalt materials both adsorb nearly 30 percent water by weight (wt%) below 5% RH. The copper analog exhibits a significantly lower water capacity, as well as an irreversible step at 30% RH. Powder X-ray diffraction (PXRD) analysis and nitrogen adsorption experiments revealed that the copper material loses porosity and undergoes a phase change after water uptake (**Figures S1** and **S2**). Similarly, the cobalt material largely maintains its crystallinity, but loses much of its porosity after reactivation upon water sorption (**Figures S3** and **S4**). By contrast, the nickel MOF retains its crystallinity and porosity (**Figures S5** and **S6**) even after water sorption and desorption. This stability trend is in line with that
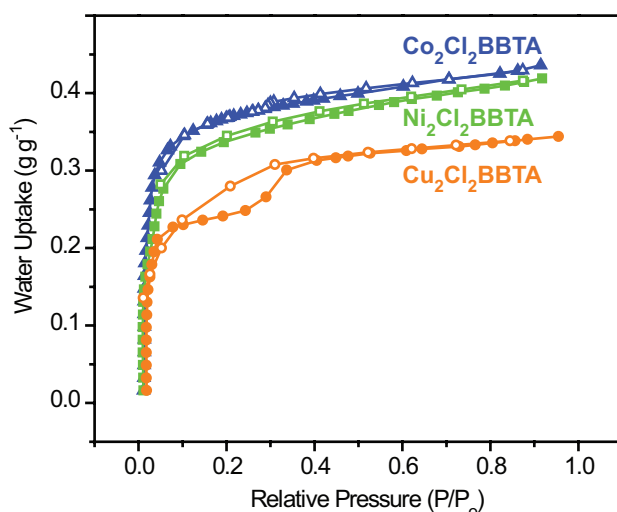

Figure 2: **Water vapor isotherms for M_2Cl_2BBTA materials**.
Adsorption (filled symbols) and desorption (open symbols) at 298 K for Co_2Cl_2BBTA (blue triangles), Ni_2Cl_2BBTA (green squares, measured at 296 K), and Cu_2Cl_2BBTA (orange circles).

previously observed for ammonia sorption in this family of materials and is the result of the kinetics of ligand exchange at the metal ion.[29]

Due to its greater stability, Ni_2Cl_2BBTA would be the more appropriate choice for a cascaded AHP. The enthalpy of water adsorption (ΔH_{ads}) in Ni_2Cl_2BBTA, determined by variable temperature water vapor sorption isotherms (**Figure S7**), is approximately 55 kJ mol^{-1} at zero coverage, nearly identical to that found for water binding to the open coordination sites of Co_2Cl_2BTDD[16] (**Figure S8**). Importantly, during pore filling of Ni_2Cl_2BBTA, ΔH_{ads} remains above 50 kJ mol^{-1}, indicating stronger across-pore hydrogen bonding interactions, likely due to confinement effects,[30,31] than those found in the larger pore Co_2Cl_2BTDD, wherein ΔH_{ads} during pore-filling is 46 kJ mol^{-1}. The variable-temperature water vapor isotherms for Ni_2Cl_2BBTA were also used to validate a characteristic curve (**Figure S9**), which converts the two independent variables that govern uptake, vapor pressure and temperature, into a single parameter related to the Gibbs free energy of adsorption (see Supplementary Information)[9,15,16] and allows extrapolation of the water loading at any temperature and pressure (**Figure S10**).

Single-Stage Heat Pump Using Ni_2Cl_2BBTA

The characteristic curve can be used to calculate water loadings in Ni_2Cl_2BBTA under conditions relevant for heat pump applications, which are in turn used to calculate the working capacity and COP. Under refrigeration II conditions (i.e. chiller output of 278 K and ambient of 303 K for 25 °C lift),[9] Ni_2Cl_2BBTA has a maximum COP of 0.70 and a volumetric working capacity of nearly 0.40 mL H_2O mL^{-1} MOF using a 400 K desorption temperature (**Figure 3A**, filled squares). This is the highest reported volumetric working capacity for any material working under Refrigeration II standardized conditions (i.e. capable of a 25 °C lift). Notably, because of the exceptional hydrophilicity of Ni_2Cl_2BBTA, the temperature lift it could achieve is primarily limited by the regeneration temperature
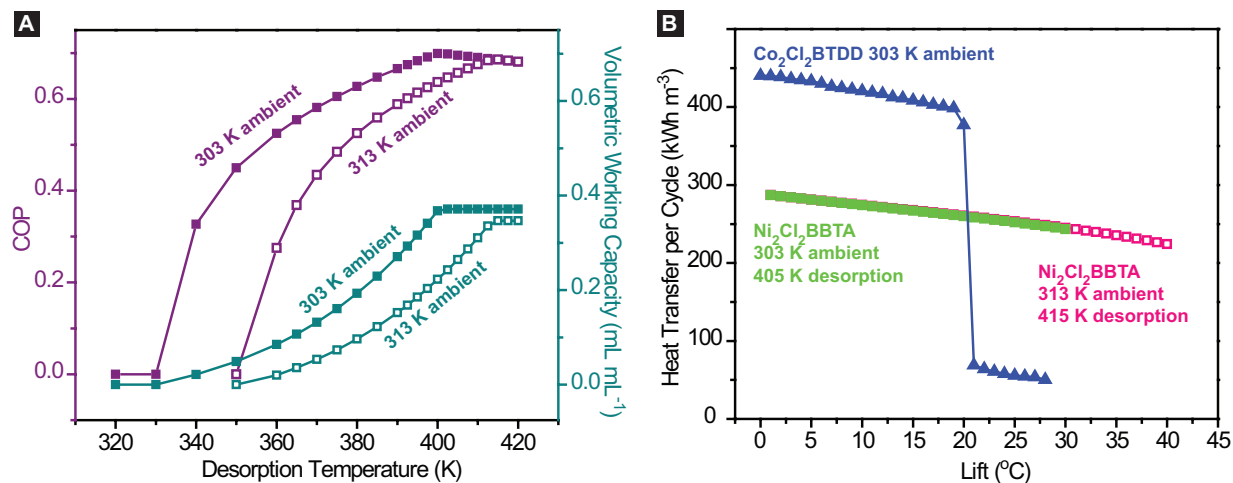

Figure 3: Single-stage heat pump figures of merit.
 A) Coefficient of Performance (purple symbols, left axis) and volumetric working capacity (aqua symbols, right axis) for Ni_2Cl_2BBTA with a chiller output temperature of 278 K and an ambient temperature of either 303 K (filled symbols, 25 °C lift) or 313 K (open symbols, 35 °C lift) as a function of desorption temperature. **B**) Heat transferred per cycle, determined by varying the evaporator (output) temperature, versus temperature lift for Ni_2Cl_2BBTA (squares) and Co_2Cl_2BTDD (blue triangles).

rather than the position of its water uptake step, which is otherwise dominant in other materials. For instance, if the ambient temperature increases to 313 K, the water-Ni_2Cl_2BBTA working pair can still produce a 278 K chiller output (35 °C lift) with only minimal decreases in the COP and working capacity (**Figure 3A**, open squares). Further, with an ambient temperature of 30 °C (303 K), Ni_2Cl_2BBTA can achieve a 30 °C lift (**Figure 3B**, filled green squares), and with an ambient temperature of 40 °C (313 K) Ni_2Cl_2BBTA can achieve a 40 °C lift with only a 10 °C increase in desorption temperature (**Figure 3B**, open pink squares).

In agreement with the characteristic curve calculations, cycling of Ni_2Cl_2BBTA between 25 °C and 150 °C at a constant vapor pressure of 4.76 mmHg (20% RH at 25 °C, well beyond the saturation RH value at this temperature) revealed an initial slight decline in uptake followed by a plateau at 0.36 g g^{-1} (**Figure S11**). We note that this is close to the vapor pressure of water ice at 0 °C, 4.585 mmHg (~20% RH at 25 °C). Impressively, nearly all of the capacity of Ni_2Cl_2BBTA, greater than 0.33 g g^{-1}, is reached below this vapor pressure (**Figure 2**). Although using water as the refrigerant makes it impossible to cool below 0 °C, the unique behaviour of Ni_2Cl_2BBTA towards water vapour highlights its potential as a desiccant in other applications such as industrial compressed air drying that require sub-zero dewpoints.[32]

Two-Stage Cascaded Heat Pump Using Ni_2Cl_2BBTA and Co_2Cl_2BTDD

In order to utilize the full potential driving force for heat transfer with Ni_2Cl_2BBTA, we devised a concept tandem cascaded heat pump cycle (**Figure 4A** and **4B**). Due to the material's exceptional affinity for water, water vapor can be adsorbed from a low temperature evaporator onto a bed of Ni_2Cl_2BBTA maintained between 104 °C and 57 °C. When combined in a tandem cycle with a material exhibiting a lower affinity for water
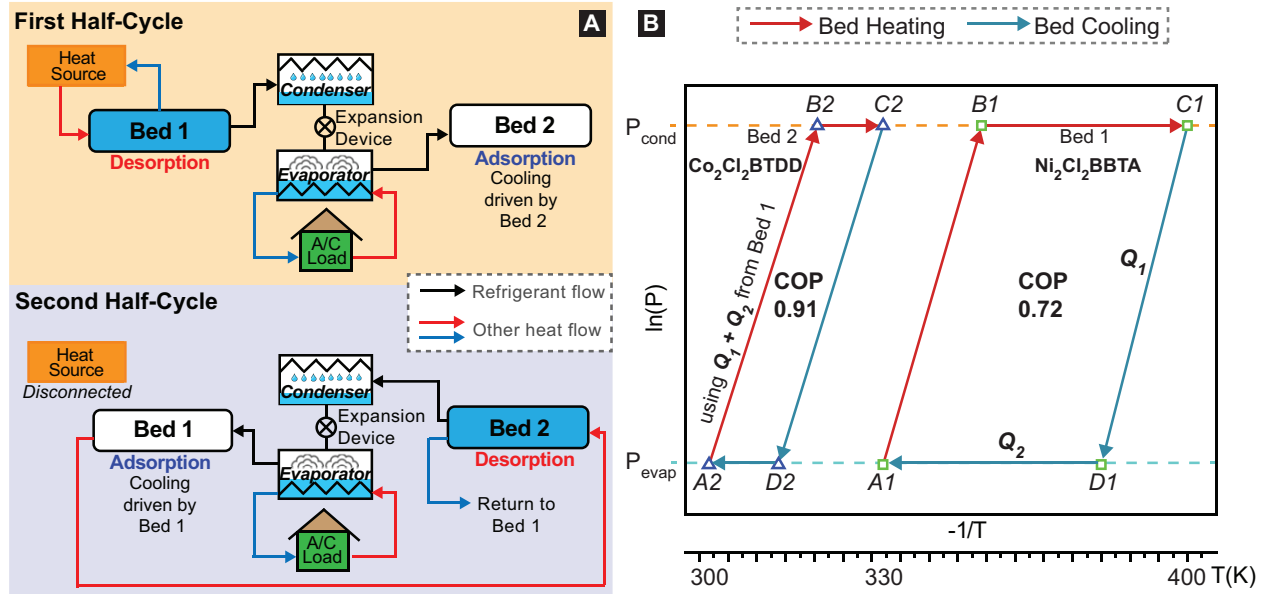

Figure 4: **Two-stage cascaded heat pump cycle diagram and thermodynamics.** **A**) Schematic of a cascaded double-effect adsorption heat pump for stationary applications. **B**) Isosteric cycle diagram of a cascaded adsorption heat pump cycle providing a 17 °C lift with evaporator at 283 K, condenser at 300 K, desorption of Co_2Cl_2BTDD at 330 K and desorption of Ni_2Cl_2BBTA at 400 K.
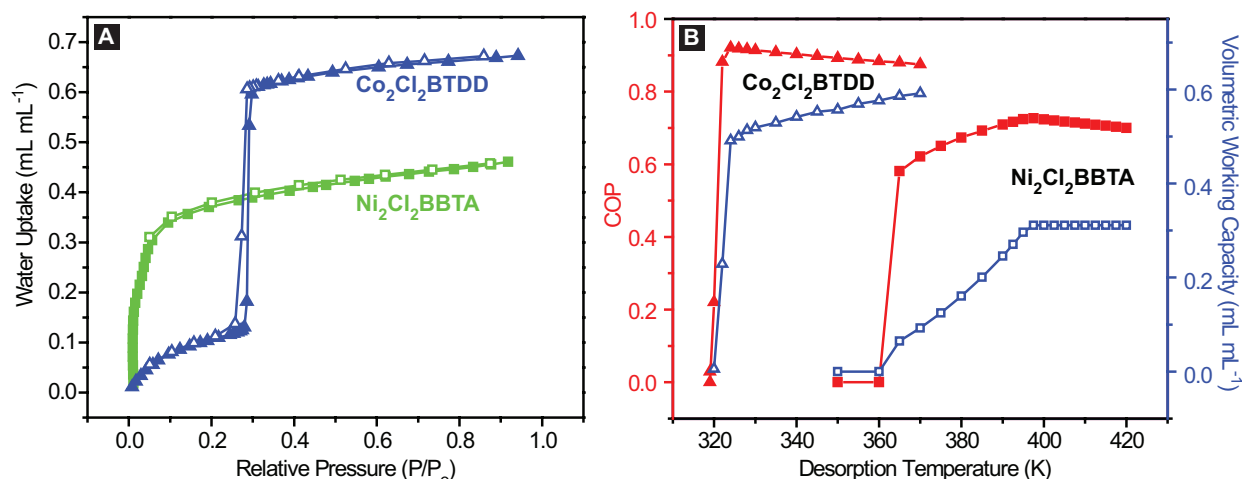
Figure 5: **Two-stage cascaded heat pump figures of merit.**
A) Water vapor adsorption (filled symbols) and desorption (open symbols) in volumetric units at 298 K for Co_2Cl_2BTDD (blue triangles) and Ni_2Cl_2BBTA (green squares) **B)** Coefficient of Performance (open symbols, left axis) and volumetric working capacity (filled symbols, right axis) for Co_2Cl_2BTDD (blue triangles) and Ni_2Cl_2BBTA (green squares) using an evaporator temperature of 283 K and an ambient temperature of 300 K, with a minimum bed temperature during adsorption of 330 K for Ni_2Cl_2BBTA, as a function of desorption temperature.

vapor, for instance the larger-pore Co_2Cl_2BTDD, the sensible heat (Q_1) as well as the energy from ΔH_{ads} (Q_2) in the small-pore Ni_2Cl_2BBTA (Bed 1) at elevated temperature can be used to completely regenerate the larger-pore Co_2Cl_2BTDD (Bed 2). Both adsorbent beds can be paired with the same evaporator and condenser, at temperatures of 10 °C and 27 °C respectively (17 °C lift). The minimum adsorption temperature of Bed 2 (Co_2Cl_2BTDD) would be that of the condenser, 27 °C, and it would be regenerated at 57 °C with waste heat from Bed 1 (Ni_2Cl_2BBTA). In turn, Bed 1 would operate at a minimum adsorption temperature of 57 °C and be regenerated by an external heat source at 127 °C. This configuration is ideal for the application of district air conditioning for buildings (**Figure 4A**).

Altogether, Ni_2Cl_2BBTA and Co_2Cl_2BTDD combine for a cascaded double-effect AHP cycle in which the input thermal energy for regeneration is effectively used twice, once at 127 °C to regenerate the small pore MOF, and again at 57 °C to regenerate the large-pore MOF. In this tandem configuration, Co_2Cl_2BTDD has a working capacity of 0.52 mL mL^{-1} and a COP of 0.91 when regenerated at 57 °C, whereas Ni_2Cl_2BBTA has a working capacity of 0.31 mL mL^{-1} and a COP of 0.72 when regenerated at 127 °C (**Figure 5B**). Because the COP of the cascading pump is the sum of the COPs for the constituent cycles, the ideal system COP for the combination presented here is 1.63.

The thermodynamic cycle is diagrammed in process flow in **Figure 4A** and in a tandem isosteric cycle in **Figure 4B**. Beginning with a saturated bed of Ni_2Cl_2BBTA (Bed 1, point *A1*) and an empty bed of Co_2Cl_2BTDD (Bed 2, point *C2*), Bed 1 undergoes isosteric heating to point *B1* and its vapor pressure increases from 9.5 mmHg (the pressure of the evaporator) to 26.6 mmHg (the pressure of the condenser). At the same time, Bed 2 undergoes isosteric cooling from point *C2* to point *D2*. Subsequently, Bed 1 is further heated while connected to the condenser for isobaric desorption to point *C1*, while Bed 2 is connected to the evaporator and undergoes isobaric adsorption to point *A2*. At this point the roles of the beds

reverse in the second half-cycle (**Figure 4A**). Bed 1 is cooled isosterically to point *D1*, connected to the evaporator, and undergoes isobaric adsorption back to *A1* while the sensible heat Q_1 and the heat of adsorption Q_2 from this process are used to regenerate Bed 2, moving from *A2* to *B2* and finally *C2* (**Figure 4B**).

Discussion

The foregoing results are the first example of materials with thermodynamically-tuned, steep, and non-overlapping water isotherms (**Figure 5A**) employed in a cascaded adsorption cycle, which enables significantly greater thermal efficiency by reducing the required temperature swings and minimizing the dead thermal mass. For example, using conventional sorbents, which, due to overlapping isotherms neccesitate employing different refigerants for each stage, an AHP with a cooling COP of 1 requires a three-stage cascade with a source temperature of 220 °C.[14] Additionally, previous screening of sorbent-sorbate pairs for tandem heat pumps found theoretical maxima for COP of 1.15 for a tandem activated carbon-methanol and zeolite-water cycle.[13] By contrast, using MOFs with stepped water isotherms tuned by pore size, we demonstrate a record ideal COP of 1.63, over 150% higher than the previous best, notably decreasing complexity by using water as the sole refrigerant, and employing a much lower source temperature of 127 °C.

Triazolate MOFs are uniquely suited to water vapor isotherm engineering by virtue of their exceptional stability as well as their hydrophilic chains of metals exhibiting open coordination sites. The microporous BBTA MOFs adsorb water vapor near 0% RH. This unusually high hydrophilicity engenders a high driving force for heat transfer. Compared to other materials capable of generating a 25 °C lift, Ni_2Cl_2BBTA has the greatest uptake capacity and positions it as a key material for the hot adsorption bed of a cascaded adsorption heat pump. When used in tandem, Ni_2Cl_2BBTA and Co_2Cl_2BTDD combine for an unprecedented COP of 1.63, which can be achieved using an accessible low driving temperature of only 127 °C. The ability to provide continuous cooling with simultaneously high COP and low source temperatures is a significant advance over the state-of-the-art. This work moves sustainable adsorption heat pumps using water as a refrigerant closer to widespread adoption.

Experimental Procedures

Water vapor adsorption isotherms were measured by a volumetric method using a Micromeritics ASAP 2020 gas sorption analyzer with a vapor dose option and a heated manifold. A typical sample of ca. 40 mg of metal-organic framework, pre-activated at 100°C to remove all residual solvent, was transferred in an Ar filled glovebox to a pre-weighed analysis tube. The tube with sample inside was weighed again to determine the mass of the sample. The tube was capped with a Micromeritics TranSeal, brought out of the glovebox, and transferred to the analysis port of the gas sorption analyzer. Free space correction measurements were performed using ultra-high purity He gas (UHP grade 5, 99.999% pure). Water vapor adsorption isotherms were measured using Milli-Q water. The water was degassed on the ASAP 2020 manifold prior to measurement. All analyses were performed using a water bath held at constant temperature with a recirculating chiller. The manifold was held 15 °C above the temperature of the sample water bath, and the vapor dosing tube was held 10 °C above the temperature of the sample water bath. Oil-free vacuum pumps were used to prevent contamination of sample or feed gases.

Acknowledgements

Author Contributions

AJR and MD conceived of experiments. AJR and AMW synthesized materials and performed experiments. AJR, SR, HK, and ENW designed and calculated parameters for the cascaded thermal cycle. ADL performed cycling experiments. AJR wrote the initial manuscript. AJR, AMW, SR, HK, ADL, ENW, and MD revised the manuscript.

Declaration of Interests

AJR and MD are inventors on a patent pertaining to the materials discussed herein.

References

[1]   U.S. Energy Information Agency. Annual Energy Outlook 2015 with Projections to 2040. Washington, DC: 2015.

[2]   Reese A. Slow coolant phaseout could worsen warming: As countries crank up the AC, emissions of potent greenhouse gases are likely to skyrocket. Science 2018;359:1084. doi:10.1126/science.359.6380.1084.

[3]   Critoph RE. Evaluation of alternative refrigerant-adsorbent pairs for refrigeration cycles. Appl Therm Eng 1996;16:891–900. doi:10.1016/1359-4311(96)00008-7.

[4]   Jeremias F, Fröhlich D, Janiak C, Henninger SK. Advancement of sorption-based heat transformation by a metal coating of highly-stable, hydrophilic aluminium fumarate MOF. RSC Adv 2014;4:24073. doi:10.1039/c4ra03794d.

[5]   Narayanan S, Yang S, Kim H, Wang EN. Optimization of adsorption processes for climate control and thermal energy storage. Int J Heat Mass Transf 2014;77:288–300. doi:10.1016/j.ijheatmasstransfer.2014.05.022.

[6]   Greenblatt JB, Wei M. Assessment of the climate commitments and additional mitigation policies of the United States. Nat Clim Chang 2016;6:1090–3.

[7]   Anderson JB, Catania G a, Alley RB, Anandakrishnan S, Dupont TK, Pollard D, et al. CO2 Is Not the Only Gas. Science 2007;315:1804–5.

[8]   McLinden MO, Brown JS, Brignoli R, Kazakov AF, Domanski PA. Limited options for low-global-warming-potential refrigerants. Nat Commun 2017;8:1–9. doi:10.1038/ncomms14476.

[9]   De Lange MF, Verouden KJFM, Vlugt TJH, Gascon J, Kapteijn F. Adsorption-Driven Heat Pumps: The Potential of Metal-Organic Frameworks. Chem Rev 2015;115:12205–50. doi:10.1021/acs.chemrev.5b00059.

[10]   Ehrenmann J, Henninger SK, Janiak C. Water Adsorption Characteristics of MIL-101 for Heat-Transformation Applications of MOFs. Eur J Inorg Chem 2011;2011:471–4. doi:10.1002/ejic.201001156.

[11]   Canivet J, Bonnefoy J, Daniel C, Legrand A, Coasne B, Farrusseng D. Structure–property relationships of water adsorption in metal–organic frameworks. New J Chem 2014;38:3102. doi:10.1039/c4nj00076e.

[12]   Küsgens P, Rose M, Senkovska I, Fröde H, Henschel A, Siegle S, et al. Characterization of metal-organic frameworks by water adsorption. Microporous Mesoporous Mater

2009;120:325–30. doi:10.1016/j.micromeso.2008.11.020.

[13] Meunier F. Theoretical Performances of Solid Adsorbent Cascading Cycles Using the Zeolite-Water and Active Carbon-Methanol Pairs: Four Case Studies. J Heat Recover Syst 1986;6:491–8.

[14] Douss N, Meunier F. Experimental study of cascading adsorption cycles. Chem Eng Sci 1989;44:225–35. doi:10.1016/0009-2509(89)85060-2.

[15] Cadiau A, Lee JS, Damasceno Borges D, Fabry P, Devic T, Wharmby MT, et al. Design of Hydrophilic Metal Organic Framework Water Adsorbents for Heat Reallocation. Adv Mater 2015;27:4775–80. doi:10.1002/adma.201502418.

[16] Rieth AJ, Yang S, Wang EN, Dincă M. Record Atmospheric Fresh Water Capture and Heat Transfer with a Material Operating at the Water Uptake Reversibility Limit. ACS Cent Sci 2017;3:668–72. doi:10.1021/acscentsci.7b00186.

[17] Jeremias F, Khutia A, Henninger SK, Janiak C. MIL-100(Al, Fe) as water adsorbents for heat transformation purposes—a promising application. J Mater Chem 2012;22:10148. doi:10.1039/c2jm15615f.

[18] Wade CR, Corrales-Sanchez T, Narayan TC, Dincă M. Postsynthetic tuning of hydrophilicity in pyrazolate MOFs to modulate water adsorption properties. Energy Environ Sci 2013;6:2172. doi:10.1039/c3ee40876k.

[19] Wright AM, Rieth AJ, Yang S, Wang E, Dinca M. Precise control of pore hydrophilicity enabled by post-synthetic cation exchange in metal-organic frameworks. Chem Sci 2018;9:3856. doi:10.1039/C8SC00112J.

[20] Akiyama G, Matsuda R, Sato H, Hori A, Takata M, Kitagawa S. Effect of functional groups in MIL-101 on water sorption behavior. Microporous Mesoporous Mater 2012;157:89–93. doi:10.1016/j.micromeso.2012.01.015.

[21] Jeremias F, Lozan V, Henninger SK, Janiak C. Programming MOFs for water sorption: amino-functionalized MIL-125 and UiO-66 for heat transformation and heat storage applications. Dalton Trans 2013;42:15967–73. doi:10.1039/c3dt51471d.

[22] Canivet J, Fateeva A, Guo Y, Coasne B, Farrusseng D. Water adsorption in MOFs: fundamentals and applications. Chem Soc Rev 2014;43:5594–617. doi:10.1039/c4cs00078a.

[23] Coasne B, Gubbins KE, Pellenq RJM. Temperature effect on adsorption/desorption isotherms for a simple fluid confined within various nanopores. Adsorption 2005;11:289–94. doi:10.1007/s10450-005-5939-y.

[24] Jasuja H, Zang J, Sholl DS, Walton KS. Rational tuning of water vapor and CO 2 adsorption in highly stable Zr-based MOFs. J Phys Chem C 2012;116:23526–32. doi:10.1021/jp308657x.

[25] Burtch NC, Jasuja H, Walton KS. Water Stability and Adsorption in Metal − Organic Frameworks. Chem Rev 2014;114:10575–612. doi:10.1021/cr5002589.

[26] Rieth AJ, Tulchinsky Y, Dincă M. High and Reversible Ammonia Uptake in Mesoporous Azolate Metal-Organic Frameworks with Open Mn, Co, and Ni Sites. J Am Chem Soc 2016;138:9401–4. doi:10.1021/jacs.6b05723.

[27] Liao P-Q, Li X-Y, Bai J, He C-T, Zhou D-D, Zhang W-X, et al. Drastic enhancement of catalytic activity via post-oxidation of a porous MnII triazolate framework. Chem - A Eur J 2014;20:11303–7. doi:10.1002/chem.201403123.

[28] Liao P-Q, Chen H, Zhou D-D, Liu S-Y, He C-T, Rui Z, et al. Monodentate hydroxide as a super strong yet reversible active site for CO 2 capture from high-humidity flue gas.

Energy Environ Sci 2015;8:1011–6. doi:10.1039/C4EE02717E.

[29]   Rieth AJ, Dincă M. Controlled Gas Uptake in Metal-Organic Frameworks with Record Ammonia Sorption. J Am Chem Soc 2018;140:3461–6. doi:10.1021/jacs.8b00313.

[30]   Derouane EG, Chang CD. Confinement effects in the adsorption of simple bases by zeolites. Microporous Mesoporous Mater 2000;35–36:425–33. doi:10.1016/S1387-1811(99)00239-5.

[31]   de Lange MF, van Velzen BL, Ottevanger CP, Verouden KJFM, Lin L-C, Vlugt TJH, et al. Metal–Organic Frameworks in Adsorption-Driven Heat Pumps: The Potential of Alcohols as Working Fluids. Langmuir 2015;31:12783–96. doi:10.1021/acs.langmuir.5b03272.

[32]   Carter JW, Wyszynski ML. The pressure swing adsorption drying of compressed air. Chem Eng Sci 1983;38:1093–9. doi:10.1016/0009-2509(83)80030-X.

Supplemental Information

Tunable Metal-Organic Frameworks Enable High Efficiency Cascaded Adsorption Heat Pumps

Adam J. Rieth[1], Ashley M. Wright[1], Sameer Rao[2], Hyunho Kim[2], Alina D. LaPotin[2], Evelyn N. Wang[2], and Mircea Dincă[1]*

[1]Department of Chemistry, Massachusetts Institute of Technology, 77 Mass. Ave. Cambridge, Massachusetts, 02139, United States.

[2]Department of Mechanical Engineering, Massachusetts Institute of Technology, 77 Mass. Ave. Cambridge, Massachusetts, 02139, United States.

*Corresponding Author: mdinca@mit.edu

Materials and Methods

$CuCl_2 \cdot 4H_2O$ (98%, Strem Chemicals), $CoCl_2 \cdot 6H_2O$ (99.9%, Alfa Aesar), $NiCl_2 \cdot 6H_2O$ (Strem Chemicals), HCl (32-35%, BDH – VWR Analytic) methanol (99.9%, VWR), *N,N*-dimethylformamide (99.8%, Millipore), ethanol (ACS grade, Mallinckrodt) were used as received.

Powder X-ray diffraction (PXRD) patterns were recorded with a Bruker Advance II diffractometer equipped with a $\theta/2\theta$ Bragg-Brentano geometry and Ni-filtered CuKα radiation (Kα_1 = 1.5406 Å, Kα_2 = 1.5444 Å, Kα_1/ Kα_2 = 0.5). The tube voltage and current were 40 kV and 40 mA, respectively. Samples for PXRD were prepared by placing a thin layer of the appropriate material on a zero-background silicon crystal plate.

Nitrogen adsorption isotherms were measured by a volumetric method using a Micromeritics ASAP 2020 gas sorption analyzer. A typical sample of ca. 40 mg of metal-organic framework, pre-activated at 100°C to remove all residual solvent, was transferred in an Ar filled glovebox to a pre-weighed analysis tube. The tube with sample inside was weighed again to determine the mass of the sample. The tube was capped with a Micromeritics TranSeal, brought out of the glovebox, and transferred to the analysis port of the gas sorption analyzer. Free space correction measurements were performed using ultra-high purity He gas (UHP grade 5, 99.999% pure). Nitrogen isotherms were measured using UHP grade nitrogen. All nitrogen analyses were performed using a liquid nitrogen bath at 77 K. Oil-free vacuum pumps were used to prevent contamination of sample or feed gases.

Water vapor adsorption cycling experiments were performed using a Surface Measurement Systems DVS Adventure dynamic gravimetric water sorption analyzer. A typical sample of ca. 5 mg of MOF, pre-activated at 150 °C, but later exposed to air, was loaded into the microbalance. The instrument was set to deliver a constant vapor pressure of 4.76 mmHg. The baseline mass of the sample was measured over 2 hours at the desorption temperature. The sample was then cycled between the adsorption temperature, and the desorption temperature 10 times. The sample mass was measured once per minute. Heating and cooling ramp rates were 1 °C per minute. The instrument switched to the next cycle when the change in mass per minute was less than 0.02 %.

M_2Cl_2BBTA MOFs were synthesized and activated according to previously published procedures.[1–3]

Calculation of the Characteristic Curve for Ni$_2$Cl$_2$BBTA.

In order to make the loading dependent on only one free variable (A, energy) rather than two (P,T), we constructed a characteristic curve.[4–6] The energy parameter used is the adsorption potential (A), which is the Gibbs free energy of adsorption with inverse sign:

$$A = RT \ln\left(\frac{p_o(T)}{p}\right)$$

p_o is the saturation vapor pressure of the working fluid at the temperature of analysis, p is the pressure at each loading value, R is the ideal gas constant, and T is the analysis temperature.

Isotherms measured at different temperatures should collapse onto a single characteristic curve. Water isotherms for Ni$_2$Cl$_2$BBTA were measured at 283 K, 288 K, and 296 K (Figure S7). After calculating the characteristic curve using each of these isotherms, it is evident that they all collapse into a single characteristic curve (Figure S9) confirming the validity of the characteristic curve model.

The characteristic curve for the highest temperature 296 K isotherm, that closest to the temperatures typically found in AHP systems, was then fitted with a simple cubic equation in order to easily extrapolate the water loading for any A value (Figure S10)

Calculation of the Heat Transferred per cycle as a Function of Temperature Lift for the Water-Ni$_2$Cl$_2$BBTA working pair (Figure 3B).

To determine temperature lift, the evaporator temperature, which determines the vapor pressure of the water being adsorbed by the MOF, was varied while the condenser at ambient temperature (set equal to the minimum temperature of the MOF bed) was held constant at 303 K or 313 K and the desorption temperature was held constant at 405 K or 415 K. The adsorption potential was then calculated for the empty state, using the vapor pressure and temperature at desorption conditions, that is, the vapor pressure of the condenser, and the desorption temperature. The adsorption potential was also calculated for the full state, using a bed temperature of 303 K or 313 K and with the water vapor pressure allowed to vary with the condenser temperature from 273 K to 303 K or 313 K (30° or 40° lift). The adsorption potential values were then converted to loadings of water in Ni$_2$Cl$_2$BBTA by using the previously determined cubic equation fitted to the characteristic curve. The desorption loading was then subtracted from the adsorption loading to determine the net working capacity. Loading values of water per gram MOF were then converted into energy values using the enthalpy of evaporation of water (44 J g^{-1}). Gravimetric values were converted into volumetric values using the crystal density of the MOF (1.1 g cm^{-3}).

Calculation of the Coefficient of Performance for the Water- Ni$_2$Cl$_2$BBTA working pair.

The COP for cooling with a 25 °C temperature lift (Refrigeration II conditions as defined by De Lange, et. al)[6] was calculated as described in the literature.[4,5] Briefly, the COP for cooling is defined as:

$$\frac{Q_{ev}}{Q_{regen}}$$

The COP for single-stage cooling may vary between 0 and 1. Q_{ev} is the heat energy removed from the evaporator through evaporation of the working fluid, and Q_{regen} is the heat energy required to regenerate the adsorbent, including isosteric heating, of both the adsorbent and the working fluid, and isobaric desorption steps. The enthalpy of adsorption of water in Ni_2Cl_2BBTA was assumed to be 53 kJ mol^{-1} throughout the working range. This is the enthalpy of adsorption at the pore filling step (Figure S8). The heat capacity of the sorbent was assumed constant at 1 J g^{-1} K^{-1}, in accordance with the literature.[6] The relevant temperatures for the calculation for refrigeration II[6] conditions are T_{cond} = 303 K, T_{ev} = 278 K. The desorption temperature was varied. The COP for cooling applications with a 25°C or 35°C temperature lift for water in Ni_2Cl_2BBTA at varied desorption temperature is shown in Figure 3A.

Calculation of the Coefficient of Performance for the Tandem Cycle working pair.

For the tandem cycle, similar calculations as above were employed for each bed separately. The total COP for the combined tandem cycle is then the sum of the COP for each component bed.

In order to match the thermal energy available from bed 1 of Ni_2Cl_2BBTA with the required regeneration energy for bed 2, the bed sizes can be adjusted based on the relative thermal energy required for each material. For instance, moving from *C1* to *A1* (Figure 4B), Ni_2Cl_2BBTA dissipates 958 J g^{-1} of thermal energy and for regeneration from *A2* to *C2*, Co_2Cl_2BTDD requires 1997 J g^{-1}, meaning that 2.08 times as much Ni_2Cl_2BBTA than Co_2Cl_2BTDD by mass should be employed. Thus, for a 10 kg (14.4 L) bed of Co_2Cl_2BTDD, a 20.8 kg (18.9 L) bed of Ni_2Cl_2BBTA should be used, which will provide continuous cooling with a 17°C lift and an ideal COP of 1.63. Per cycle, 18300 kJ of thermal energy will be transferred for Co_2Cl_2BTDD and 14400 kJ for Ni_2Cl_2BBTA.
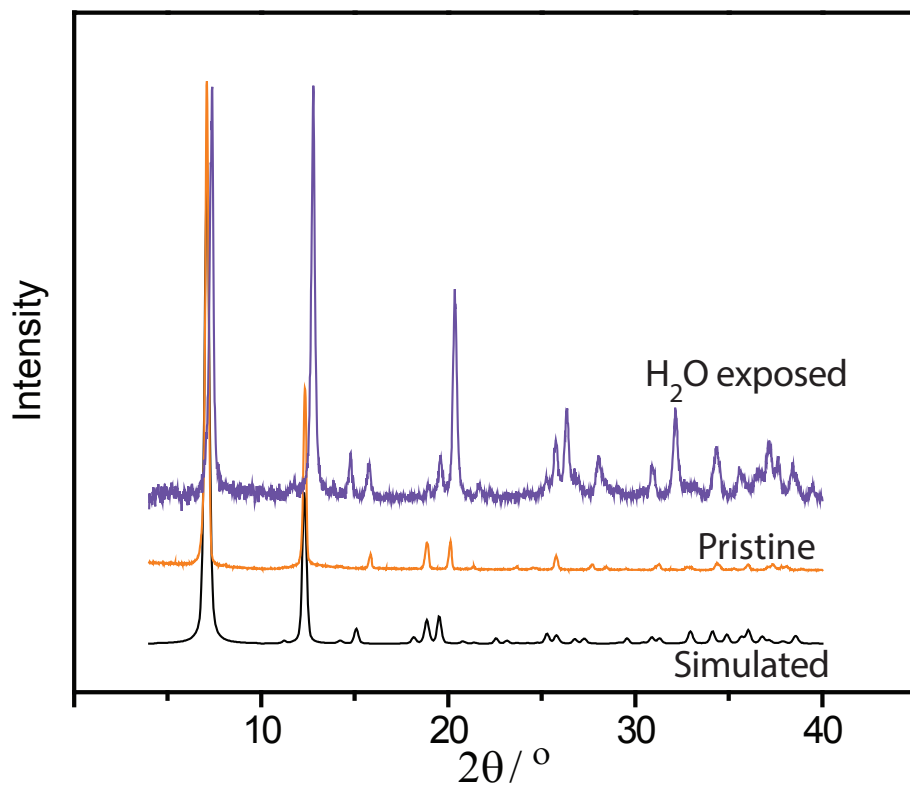
Figure S1. Powder X-ray diffraction patterns of activated Cu_2Cl_2BBTA (orange), Cu_2Cl_2BBTA after a single water isotherm at 298 K (purple), and a simulated pattern for the structure (black).
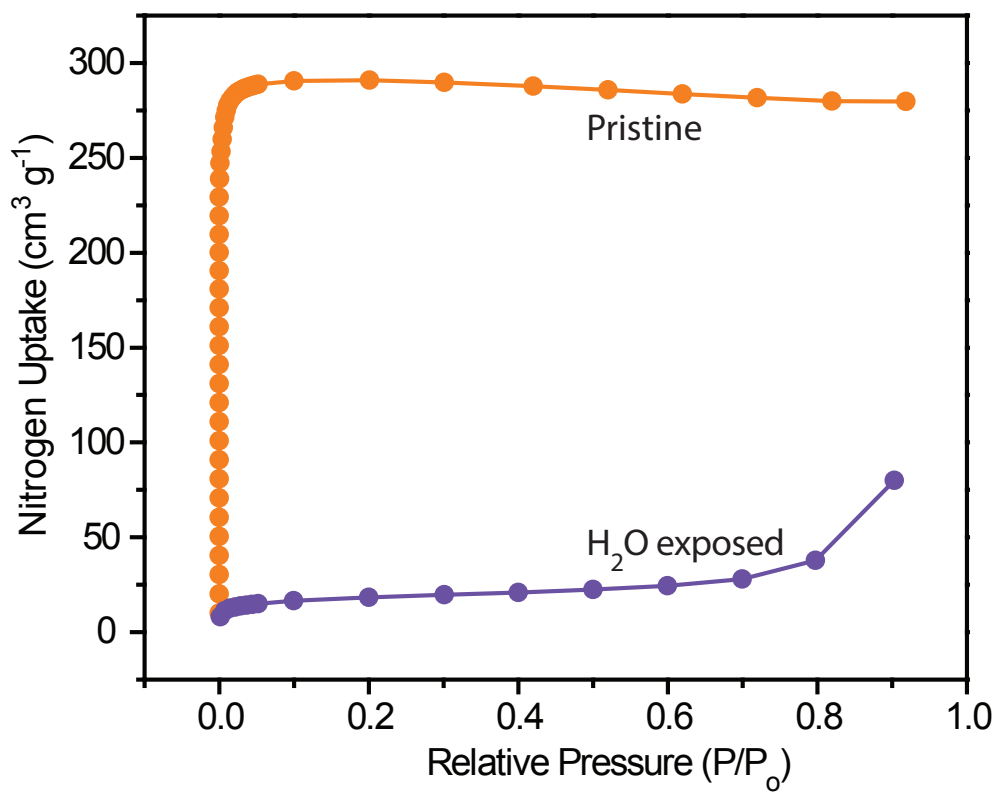
Figure S2. N_2 adsorption isotherms of activated Cu_2Cl_2BBTA (orange), and Cu_2Cl_2BBTA reactivated at 150°C after a single water isotherm at 298 K (purple).
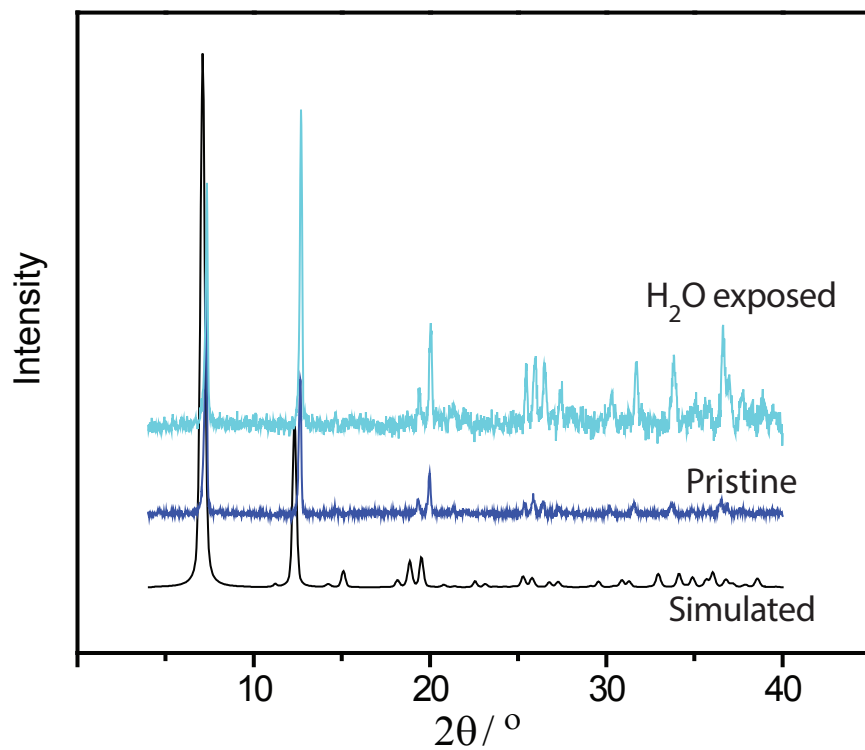
Figure S3. Powder X-ray diffraction patterns of activated Co_2Cl_2BBTA (blue), Co_2Cl_2BBTA after a single water isotherm at 298 K (light blue), and a simulated pattern for the structure (black).
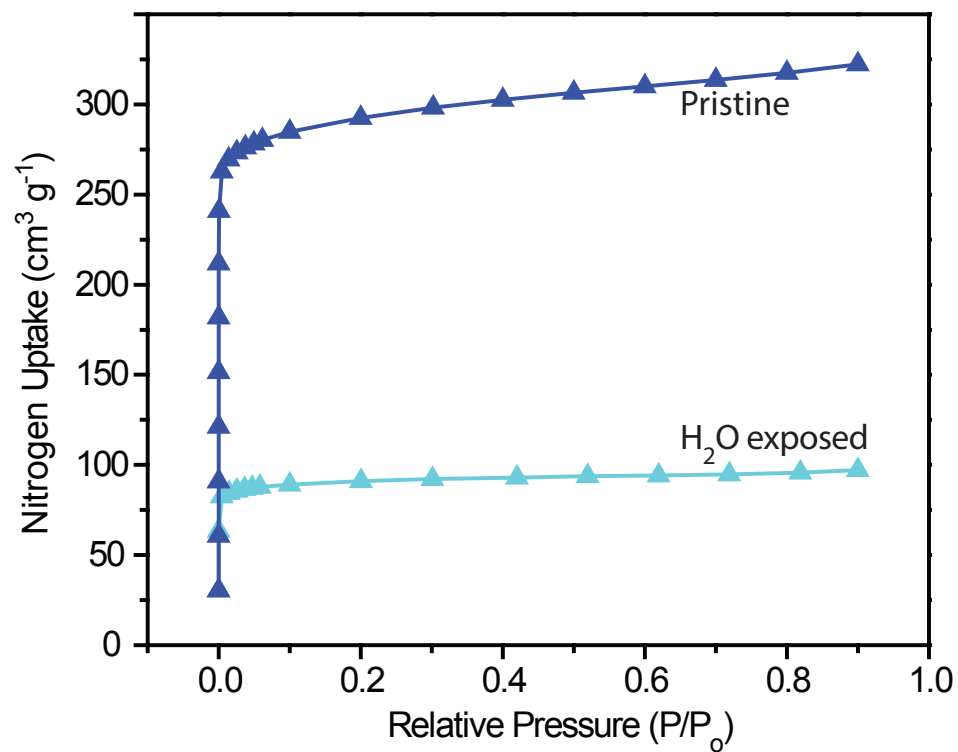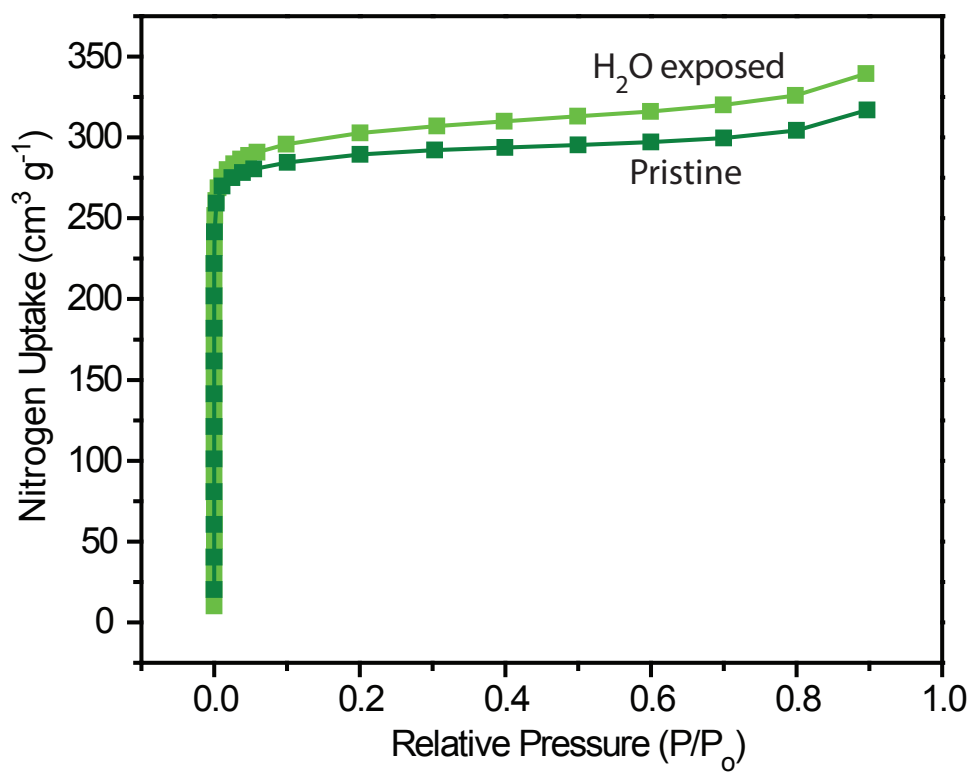
Figure S4. N_2 adsorption isotherms of activated Co_2Cl_2BBTA (blue), and Co_2Cl_2BBTA reactivated at 150°C after a single water isotherm at 298 K (light blue).
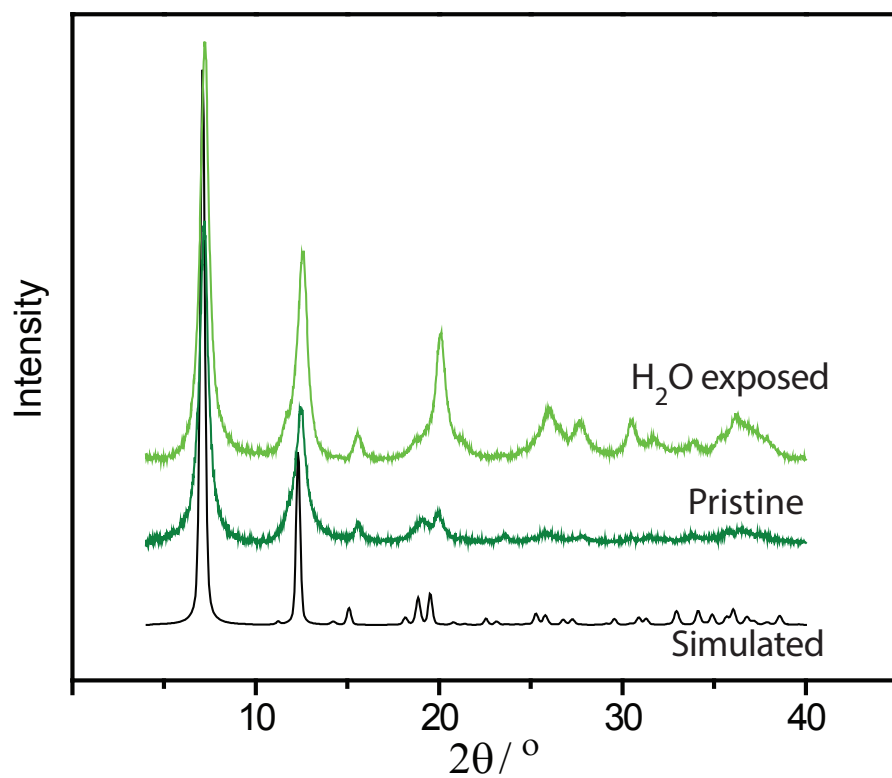
Figure S5. Powder X-ray diffraction patterns of activated Ni_2Cl_2BBTA (dark green), Ni_2Cl_2BBTA after a single water isotherm at 296 K (light green), and a simulated pattern for the structure (black).

Figure S6. N$_2$ adsorption isotherms of activated Ni$_2$Cl$_2$BBTA (dark green), and Ni$_2$Cl$_2$BBTA reactivated at 150°C after a single water isotherm at 296 K (light green).
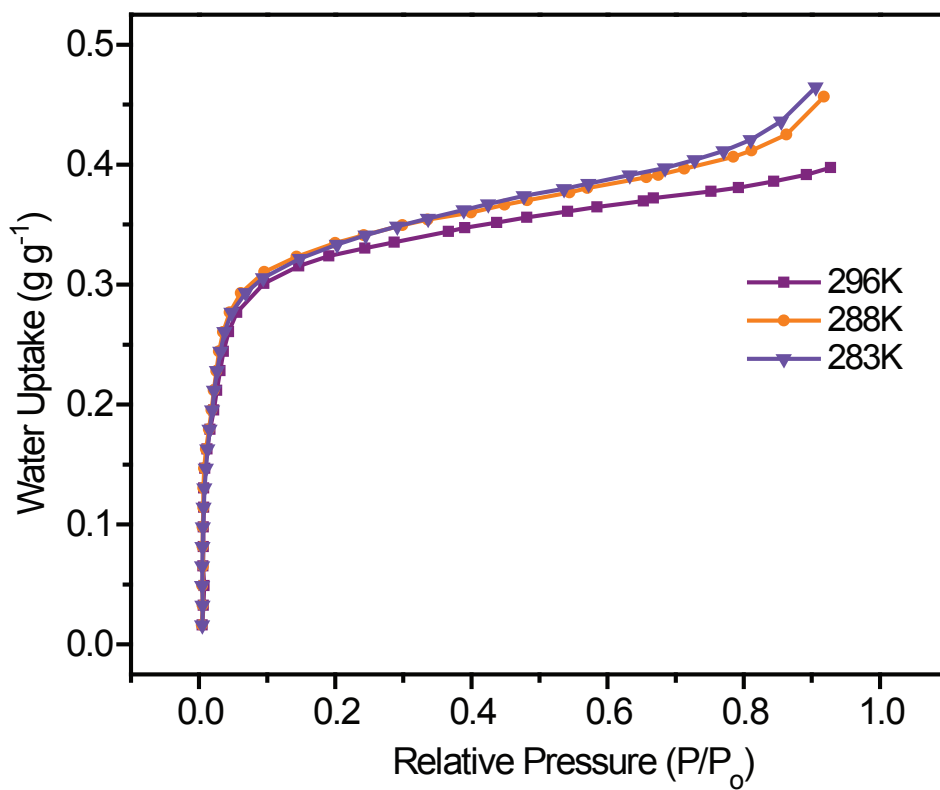
Figure S7. Variable temperature water adsorption isotherms for Ni_2Cl_2BBTA at 296 K (purple squares), 288 K (orange circles), and 283 K (blue triangles).
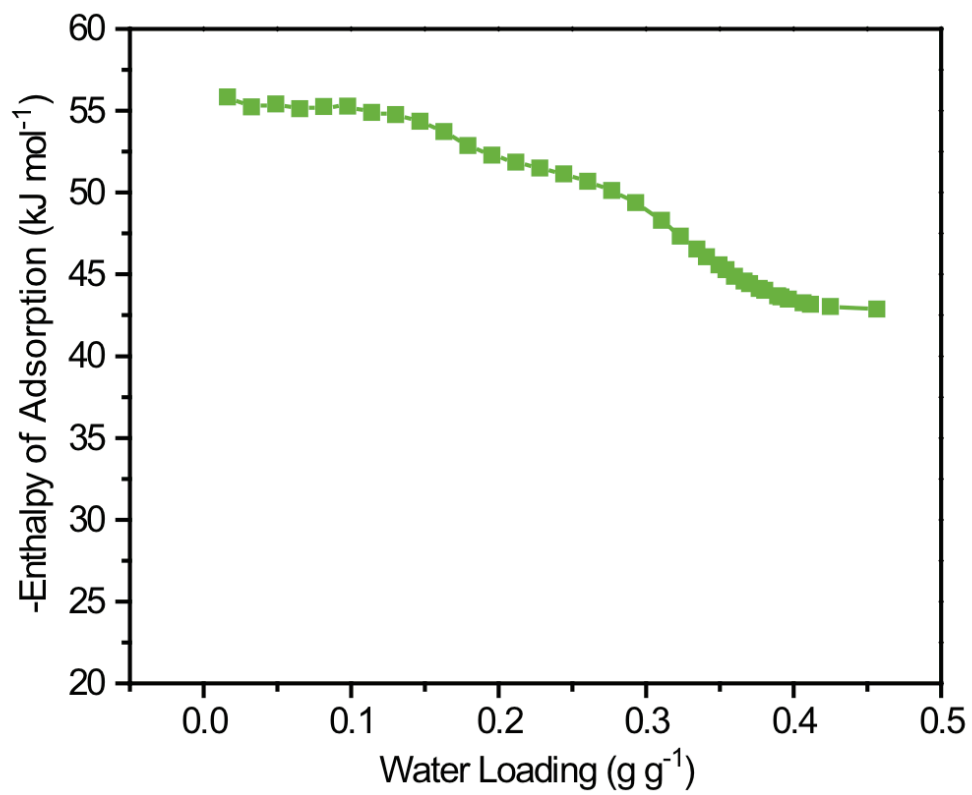
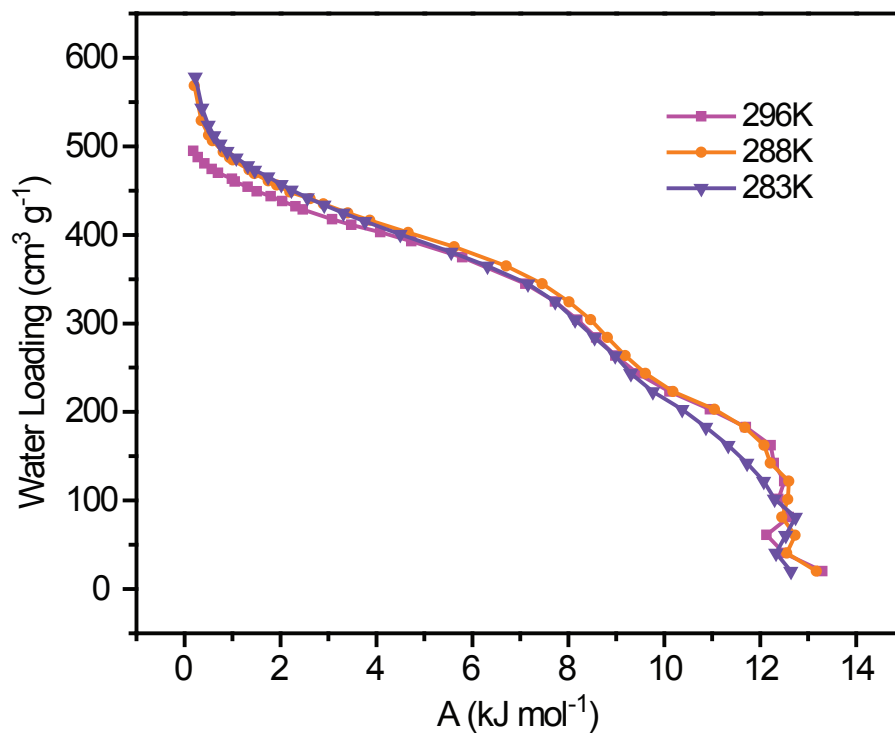**Figure S8.** The enthalpy of adsorption for water in Ni$_2$Cl$_2$BBTA versus loading.

Figure S9. Characteristic curves for water vapor adsorption in Ni_2Cl_2BBTA calculated using the isotherms at 296 K (purple squares), 288 K (orange circles), and 283 K (blue triangles). The characteristic curve is temperature invariant, justifying its usage to calculate isotherms at other temperatures relevant for AHPs.
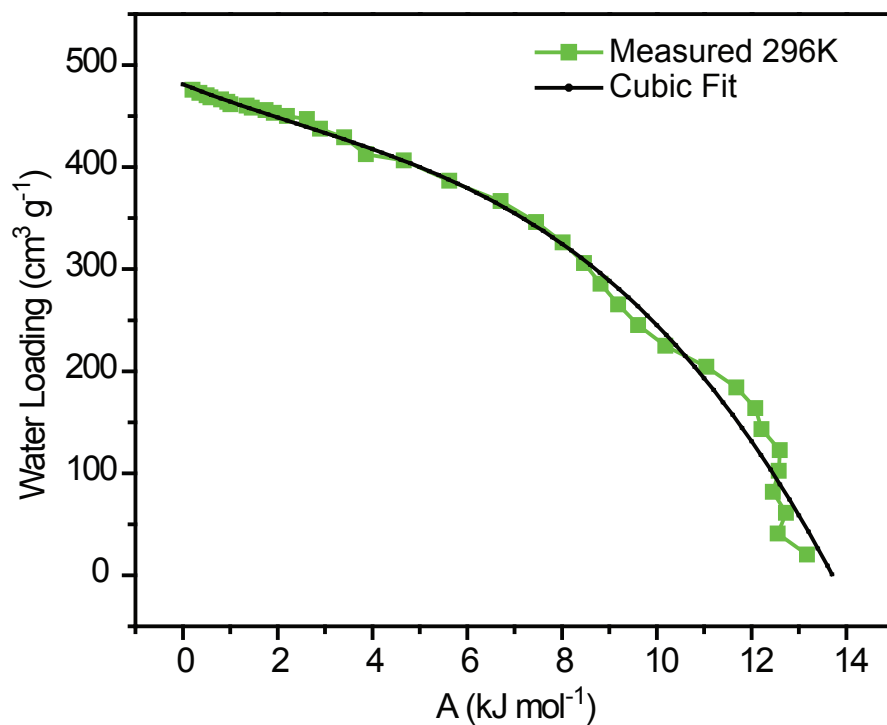
Figure S10. Cubic least-squares fit to the characteristic curve measured at 296 K. The black line is according to the equation W = -0.1869A^3+1.332A^2-18.23A+481.2. The R^2 value for the fit was 0.988 The fitted equation was used to calculate loading at temperatures and pressures relevant for AHPs.
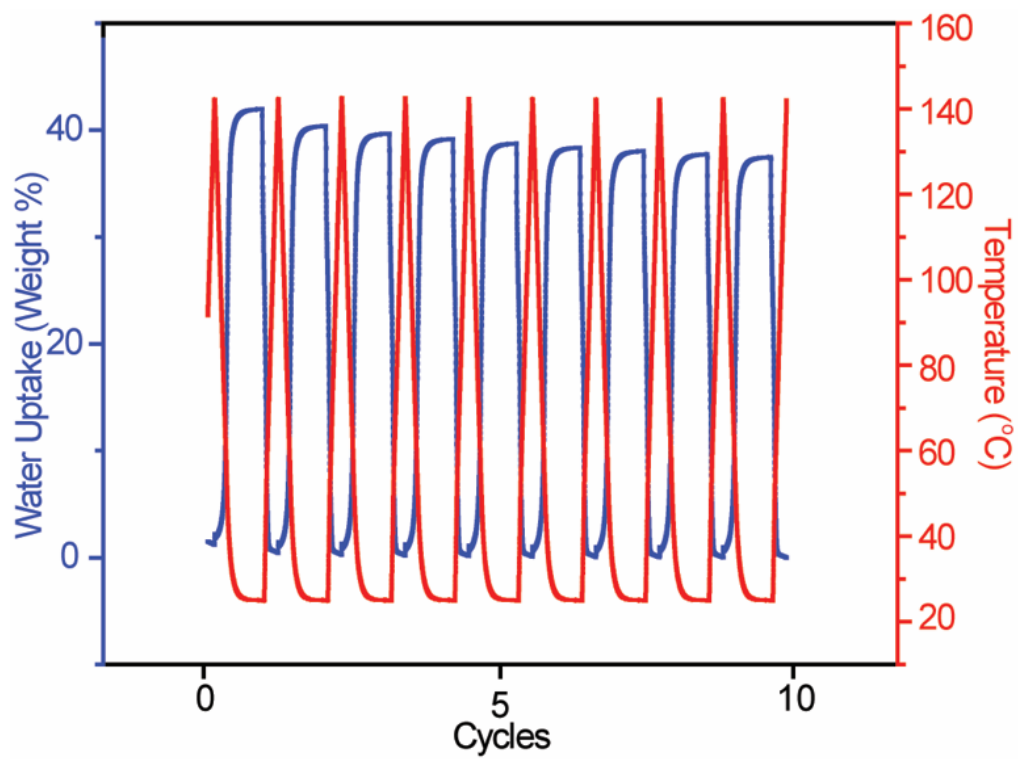
Figure S11. Temperature-swing water cycling of Ni_2Cl_2BBTA at a constant water vapor pressure of 4.76 mmHg.

References

[1]   Liao P-Q, Li X-Y, Bai J, He C-T, Zhou D-D, Zhang W-X, et al. Drastic enhancement of catalytic activity via post-oxidation of a porous MnII triazolate framework. Chem - A Eur J 2014;20:11303–7. doi:10.1002/chem.201403123.

[2]   Liao P-Q, Chen H, Zhou D-D, Liu S-Y, He C-T, Rui Z, et al. Monodentate hydroxide as a super strong yet reversible active site for CO_2 capture from high-humidity flue gas. Energy Environ Sci 2015;8:1011–6. doi:10.1039/C4EE02717E.

[3]   Rieth AJ, Dincă M. Controlled Gas Uptake in Metal-Organic Frameworks with Record Ammonia Sorption. J Am Chem Soc 2018;140:3461–6. doi:10.1021/jacs.8b00313.

[4]   de Lange MF, van Velzen BL, Ottevanger CP, Verouden KJFM, Lin L-C, Vlugt TJH, et al. Metal–Organic Frameworks in Adsorption-Driven Heat Pumps: The Potential of Alcohols as Working Fluids. Langmuir 2015;31:12783–96. doi:10.1021/acs.langmuir.5b03272.

[5]   Cadiau A, Lee JS, Damasceno Borges D, Fabry P, Devic T, Wharmby MT, et al. Design of Hydrophilic Metal Organic Framework Water Adsorbents for Heat Reallocation. Adv Mater 2015;27:4775–80. doi:10.1002/adma.201502418.

[6]   De Lange MF, Verouden KJFM, Vlugt TJH, Gascon J, Kapteijn F. Adsorption-Driven Heat Pumps: The Potential of Metal-Organic Frameworks. Chem Rev 2015;115:12205–50. doi:10.1021/acs.chemrev.5b00059.